

The *XMM–Newton* view of AGN with intermediate mass black holes

G. Miniutti^{1,2,3*}, G. Ponti², J.E. Greene⁴, L.C. Ho⁵, A.C. Fabian¹, K. Iwasawa^{6,7}

¹*Institute of Astronomy, Madingley Road, Cambridge CB3 0HA*

²*Laboratoire Astroparticule et Cosmologie (APC), UMR 7164, 10 rue A. Domon et L. Duquet, 75205 Paris Cedex 13, France*

³*Laboratorio de Astrofísica Espacial y Física Fundamental, LAEFF (CAB–CSIC–INTA), P.O. Box 78, E–28691, Villanueva de la Cañada, Madrid*

⁴*Princeton University Observatory, Princeton, NY 08544, USA*

⁵*The Observatories of the Carnegie Institution of Washington, 813 Santa Barbara St., Pasadena, CA 91101, USA*

⁶*Max–Planck–Institut für extraterrestrische Physik, Giessenbachstrasse, 85748 Garching, Germany*

⁷*INAF – Osservatorio Astronomico di Bologna, Via Ranzani 1, I–40127 Bologna, Italy*

7 November 2018

ABSTRACT

We have observed with *XMM–Newton* four radiatively efficient active type 1 galaxies with black hole masses $< 10^6 M_{\odot}$, selected optically from the Sloan Digital Sky Survey and previously detected in the Rosat All Sky Survey. Their X–ray spectra closely resemble those of more luminous Seyferts and quasars, powered by accretion onto much more massive black holes and none of the objects is intrinsically absorbed by cold matter totally covering the source. We show here that their soft X–ray spectrum exhibits a soft excess with the same characteristics as that observed ubiquitously in radio–quiet Seyfert 1 galaxies and type 1 quasars, both in terms of temperatures and strength. This is highly surprising because the small black hole mass of these objects should lead to a thermal disc contribution in the soft X–rays and not in the UV (as for more massive objects) with thus a much more prominent soft X–ray excess. Moreover, even when the soft X–ray excess is modelled with a pure thermal disc, its luminosity turns out to be much lower than that expected from accretion theory for the given temperature. While alternative scenarios for the nature of the soft excess (namely smeared ionized absorption and disc reflection) cannot be distinguished on a pure statistical basis, we point out that the absorption model produces a strong correlation between absorbing column density and ionization state, which may be difficult to interpret and is most likely spurious. Moreover, as pointed out before by others, absorption must occur in a fairly relativistic wind which is problematic, especially because of the enormous implied mass outflow rate. As for reflection, it does only invoke standard ingredients of any accretion model for radiatively efficient sources such as a hard X–rays source and a relatively cold (though partially ionized) accretion disc, and therefore seems the natural choice to explain the soft excess in most (if not all) cases. The reflection model is also consistent with the additional presence of a thermal disc component with the theoretically expected temperature (although, again, with smaller–than–expected total luminosity). We also studied in some detail the X–ray variability properties of the four objects. The observed active galaxies are among the most variable in X–rays and their excess variance is among the largest. This is in line with their relatively small black hole mass and with expectations from simple power spectra models.

Key words: galaxies: active – X-rays: galaxies

1 INTRODUCTION

Two families of black holes have been observed so far: stellar–mass black holes are seen in X–ray binaries, while black holes with masses 10^6 – $10^9 M_{\odot}$ are ubiquitous in the centers of galaxies, sometimes revealing themselves as Active Galactic Nuclei (AGN). The large mass gap between the two families is still scarcely pop-

ulated. Dynamical evidence for a black hole with mass $\sim 1.7 \times 10^4 M_{\odot}$ has been reported in the G1 globular cluster (Gebhardt, Rich & Ho 2005) and a black hole with a mass of $\sim 4 \times 10^4 M_{\odot}$ may be present in Omega Centauri as well (Noyola et al. 2008). As for AGN, a limited number of low luminosity Seyfert–like active galaxies has been shown to harbour intermediate–mass black holes (IMBH, arbitrarily defined here as black holes in galaxy centers with $M_{\text{BH}} < 10^6 M_{\odot}$). NGC 4395 is a late–type spiral with no bulge component and small central stellar velocity disper-

* gminiutti@laeff.inta.es

sion (Filippenko & Ho 2003) which exhibits broad permitted optical/UV emission lines, a compact radio core, and a highly variable point-like X-ray source unambiguously pointing towards a Seyfert identification (Filippenko, Ho & Sargent 1993; Ho & Ulvestad 2001; Ho et al 2001; Vaughan et al 2005). Mass estimates from the $H\beta$ line width–luminosity relationship (Filippenko & Ho 2003) and from X-ray variability (Vaughan et al 2005) suggest a BH of $10^4 - 10^5 M_\odot$, consistent with the upper limit ($10^5 M_\odot$) inferred from the $M-\sigma$ relation, but slightly lower than the BH mass of $3.6 \times 10^5 M_\odot$, obtained through reverberation mapping (Peterson et al. 2005). The dwarf elliptical POX 52 also exhibits Seyfert 1 like broad and narrow emission lines (Kunth, Sargent & Bothun 1987; Barth et al. 2004) and the estimate of the BH mass obtained via the $H\beta$ line width–luminosity relationship and the $M-\sigma$ relationship point toward a BH of the order of $10^5 M_\odot$. The main difference in the AGN properties of the two IMBH is that NGC 4395 is a low Eddington ratio source ($< 10^{-2}$), while POX 52 appears to be radiating at nearly its maximum rate. Finally, the dwarf Seyfert 1 SDSS J160531.84+174826.1 has a relatively broad $H\alpha$ line component which suggests (via luminosity and line width) a black hole mass of $\sim 7 \times 10^4 M_\odot$ (Dong et al. 2007b).

Greene & Ho (2004) have defined a sample of 19 IMBH candidates in AGN using the first data release of the Sloan Digital Sky Survey (SDSS). Given the adopted selection criteria (low BH mass and prominent AGN-like spectrum) the sample mostly comprises objects with high Eddington ratio. The Greene & Ho work was recently extended to the fourth data release by Dong et al (2007a) and Greene & Ho (2007b) who have increased the sample of IMBH by about one order of magnitude. Interestingly, about 15 per cent of the larger sample(s) are suspected to have Eddington ratios below 10 per cent. Due to selection criteria, and with the exception of NGC 4395, all AGN with IMBH are actually radiating a very significant fraction of their Eddington luminosity. The presence of relatively low Eddington ratio sources in the new sample(s) will make it possible to investigate NGC 4395-like nuclei in the future, opening a new important window on IMBH activity.

The original smaller Greene & Ho sample (hereafter the GH sample) has been studied in the X-rays by making use of 5 ks long *Chandra* snapshot observations (Greene & Ho 2007a). The sample is characterized by X-ray luminosities in the range of $10^{41} - 10^{43} \text{ erg s}^{-1}$ in the soft 0.5–2 keV X-ray band and the soft X-ray spectral properties are consistent with those of more luminous sources harbouring more massive black holes, showing that black hole mass is certainly not one of the main drivers of soft X-rays spectral properties.

Here we report results from *XMM-Newton* 40 ks–long observations of four of the IMBHs from the GH sample which were previously detected in the Rosat All Sky Survey. The larger effective area and longer exposure of these observations with respect to the *Chandra* snapshots allow us to consider in some detail the X-ray spectral properties of these IMBH also above 2 keV, and to compare them with their more massive and more luminous counterparts (e.g. the PG quasars). Moreover, we were able to also study their X-ray variability properties filling (although with only four objects) a relatively poorly studied range in black hole masses. Very recently, the four observations we consider here have been included in a submitted work by Dewangan et al (2008). Their analysis is mainly devoted to NGC 4395 and POX 52. As for the common sources, the main difference with our work is that we focus much more our study on the spectral analysis and soft excess, exploring different possible models and interpretations, and comparing the X-ray

Table 1. Information on the observed sources and observations. The short exposure GH 12b does not allow to obtain good quality spectra above ~ 3 keV and is not considered further.

ID	$\log M_{\text{BH}}$	z	N_H^{G}	pn exp.
(1)	(2)	(3)	(4)	(5)
GH 1	5.86	0.0768	3.89	30 ks
GH 8	5.77	0.0811	2.34	34 ks
GH 12a	5.98	0.106	2.04	17 ks
GH 12b	-	-	-	3 ks
GH 12c	-	-	-	12 ks
GH 14	5.30	0.0281	2.04	19 ks

(1) Identification from Greene & Ho (2004); (2) black hole mass from Greene & Ho (2004); (3) redshift; (4) Galactic column density in units of $\times 10^{20} \text{ cm}^{-2}$; (5) Net EPIC–pn exposure used for the spectral analysis, after filtering for periods of high background.

properties of the four objects with AGN powered by accretion onto much more massive black holes.

2 XMM-NEWTON OBSERVATIONS

All observations were performed with the EPIC–pn camera operated in Full Frame mode. In Table 1 we report the source ID (see Greene & Ho 2004 for ID definition), redshift, and Galactic column density. All observations were affected by high background periods. These were removed before performing spectral analysis and the resulting net exposure is reported in Table 1. Due to high radiation affecting the observations of GH 12, the source has been observed three times (a,b, and c in Table 1 and hereafter). Spectra have been rebinned so that each energy bin contains at least 20 counts to allow us to use the χ^2 minimisation technique in spectral fitting.

3 X-RAY SPECTRA

We first consider the hard 2–10 keV band only, and we apply a simple power law model (with neutral absorption fixed at the Galactic value) to all sources and observations. In all cases, we obtain a satisfactory description of the 2–10 keV spectra although errors on the hard spectral slope are large (of the order of 20 per cent) due to the poor signal-to-noise above a few keV in most cases. The photon index in the 2–10 keV band is consistent with 1.7–1.9 in all cases, and more details on the hard spectral slope in the individual objects will be given below.

3.1 Fe emission

The 2–10 keV spectra were also inspected for the presence of iron (Fe) emission lines. The best evidence for emission lines is seen in GH 8, where the addition of a narrow ionized Fe emission line (with energy 6.6 ± 0.1 keV and equivalent width 300 ± 200 eV) produces a $\Delta\chi^2 = 8$ for 2 degrees of freedom (i.e. significant at the ~ 97 per cent level). An additional narrow emission line at 7.4 ± 0.2 (possibly associated with Ni emission) with an equivalent width of 400 ± 250 eV is also tentatively detected (also at the ~ 97 per cent level, though the large equivalent width would imply a large Ni abundance, suggesting that the line is most likely not real). Due to the low significance of these emission features, we consider their

Table 2. We apply a broken power law model to all observations in the 0.3–10 keV band. The last column in parenthesis gives the fitting result when a single power law model is fitted in the whole 0.3–10 keV band. Galactic absorption is always assumed. Fluxes (absorbed) are given in units of 10^{-13} erg cm $^{-2}$ s $^{-1}$ and luminosities (unabsorbed) in units of 10^{43} erg s $^{-1}$. The bolometric luminosity is estimated from the optical data as $L_{\text{Bol}} = 9L_{5100}$ (Greene & Ho 2004).

ID	Γ_s	Γ_h	$F_{0.5-2}$	F_{2-10}	$L_{0.5-2}$	L_{2-10}	$L_{\text{Bol}}/L_{\text{Edd}}$	χ^2/dof
GH 1	2.38 ± 0.05	$1.8^{+0.4}_{-0.6}$	2.58 ± 0.06	2.65 ± 0.06	0.43 ± 0.01	0.37 ± 0.01	1.12	308/306 (317/308)
GH 8	$2.81^{+0.03}_{-0.02}$	$1.9^{+0.2}_{-0.3}$	5.00 ± 0.08	2.59 ± 0.04	0.93 ± 0.01	0.42 ± 0.01	2.69	401/317 (417/319)
GH 12a	2.60 ± 0.05	1.9 ± 0.3	3.49 ± 0.08	2.54 ± 0.06	1.12 ± 0.02	0.72 ± 0.02	1.10	178/206 (191/208)
GH 12c	2.55 ± 0.07	$1.7^{+0.4}_{-0.5}$	3.4 ± 0.1	3.1 ± 0.1	1.09 ± 0.04	0.85 ± 0.03	1.10	178/162 (202/164)
GH 14	2.0 ± 0.1	1.5 ± 0.2	1.02 ± 0.04	1.68 ± 0.07	0.019 ± 0.001	0.029 ± 0.001	0.29	74/88 (82/90)

detection as tentative only, and we do not discuss them any further (though they are included in all subsequent fits). In all other objects an additional narrow emission line in the range 6.4 keV–6.97 keV (neutral to highly ionized Fe) does not improve the statistics significantly.

However, a narrow (< 50 eV in σ) and neutral (~ 6.4 keV) Fe emission line is ubiquitous in the spectra of AGN with typical equivalent width of ~ 100 eV (which is also anti-correlated with X-ray luminosity and Eddington ratio, see e.g. Bianchi et al 2007). We then include an unresolved Fe K α emission line (with energy fixed at 6.4 keV) in our spectral models to compute upper limits on its equivalent width. We obtain upper limits in the range of 190–550 eV in all objects, which are consistent with expectations from Bianchi et al. (2007), given the low-luminosity of our objects (typically a few times 10^{42} erg s $^{-1}$). Hence, we do not detect any neutral Fe K α emission line at 6.4 keV, but the quality of our data is not high enough to rule out that a typical Fe line is present in the hard X-ray spectra of the sources.

3.2 Broadband spectra

We then extrapolate the hard power law model to soft energies to assess whether the hard spectral shape provides an adequate description of the broadband 0.3–10 keV data. In Fig. 1 we show the result of this exercise which highlights the presence of a soft excess: the data below 1–2 keV lie in all cases above the extrapolation of the hard power law model. We then re-fitted the simple power law model described above in the whole 0.3–10 keV band and compare it with a (phenomenological) broken power law model. In Table 2 we report the spectral slopes in the soft (Γ_s) and hard (Γ_h) band for the broken power law model only (the break energy is in the 1.5–3 keV range for all sources and is not reported). The statistics for a single power law model is reported in parenthesis in the last column and its slope was found consistent with Γ_s within the errors due to the much higher signal-to-noise in the soft band. We also give the derived X-ray fluxes and luminosities in the 0.5–2 keV and in the 2–10 keV bands and the Eddington ratio $L_{\text{Bol}}/L_{\text{Edd}}$ where $L_{\text{Bol}} = 9L_{5100}$ (Greene & Ho 2004). The spectral fitting results show that the broken power law model is a better description of the broadband X-ray spectra of GH 1 (although at the 98.8 per cent level only), GH 8, and GH 12, while a single power law model is adequate for GH 14. In other words, a soft excess is detected in GH 1, GH 8 and GH 12, and not significantly present in GH 14. We note that the broken power law model is not entirely adequate to reproduce the soft excess and that results from such spectral fits should not be used to infer the significance of the soft excess detection. A blackbody representation is a better, though also phenomenological, parametrization of the soft excess (see caption of

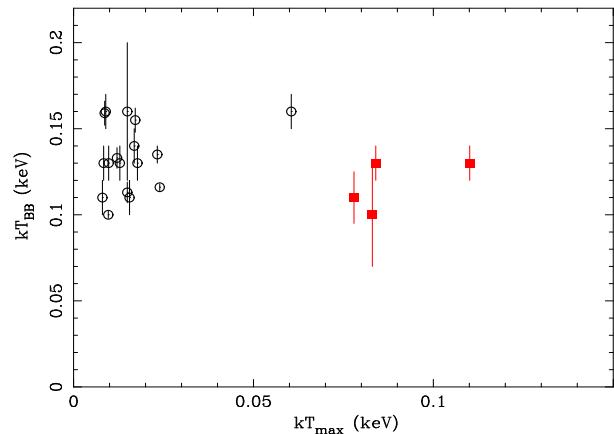


Figure 2. The observed temperature of the soft excess is plotted versus the maximum temperature expected from the accretion disc (Schwarzschild case). Filled squares are for our objects and open circles for the sample of radio-quiet PG quasars (results from Piconcelli et al 2005). For GH12, the average between observations is shown. No correlation is seen, in line with previous studies based on the PG quasars.

Fig. 1 and Table 3). We also point out that in no cases the addition of a neutral absorption component at the redshift of the source improved the statistical quality of the fit. Hence, as already mentioned by Greene & Ho (2007a) in their analysis of the *Chandra* data, neutral intrinsic absorption covering the totality of the X-ray source plays a negligible role in these sources.

The choice of the broken power law model allows to compare directly our results on the soft X-ray slope Γ_s with previous *Chandra* observations of the GH sample (Greene & Ho 2007a) which were limited to energies below ~ 3 keV due to the lack of signal-to-noise in the hard band (source GH 12 is however observed only with *XMM-Newton*). The soft spectral slopes are in good agreement with the previous *Chandra* observations (Greene & Ho 2007a), despite long-term flux variability: during the previous *Chandra* observations, GH 1 and GH 14 were 3 and 2 times brighter (respectively) than in the present *XMM-Newton* data, while GH 8 was a factor 1.4 fainter. However, the photon indexes in the 0.5–2 keV band are consistent with each other within the errors. Moreover, the values of Γ_s in Table 2 are also in line with the typical soft X-ray slope of luminous quasars (e.g. $\langle \Gamma_s \rangle \simeq 2.6 - 2.7$ in the sample of PG quasars observed by *XMM-Newton* (Porquet et al 2004; Piconcelli et al 2005). Although affected by large error bars, the hard spectral slopes are remarkably similar within each other, and also consistent with the typical 2–10 keV slope of PG quasars ($\langle \Gamma_h \rangle \simeq 1.9$). The only exception is represented by the least luminous source (GH 14), which has a flatter spectral slope in

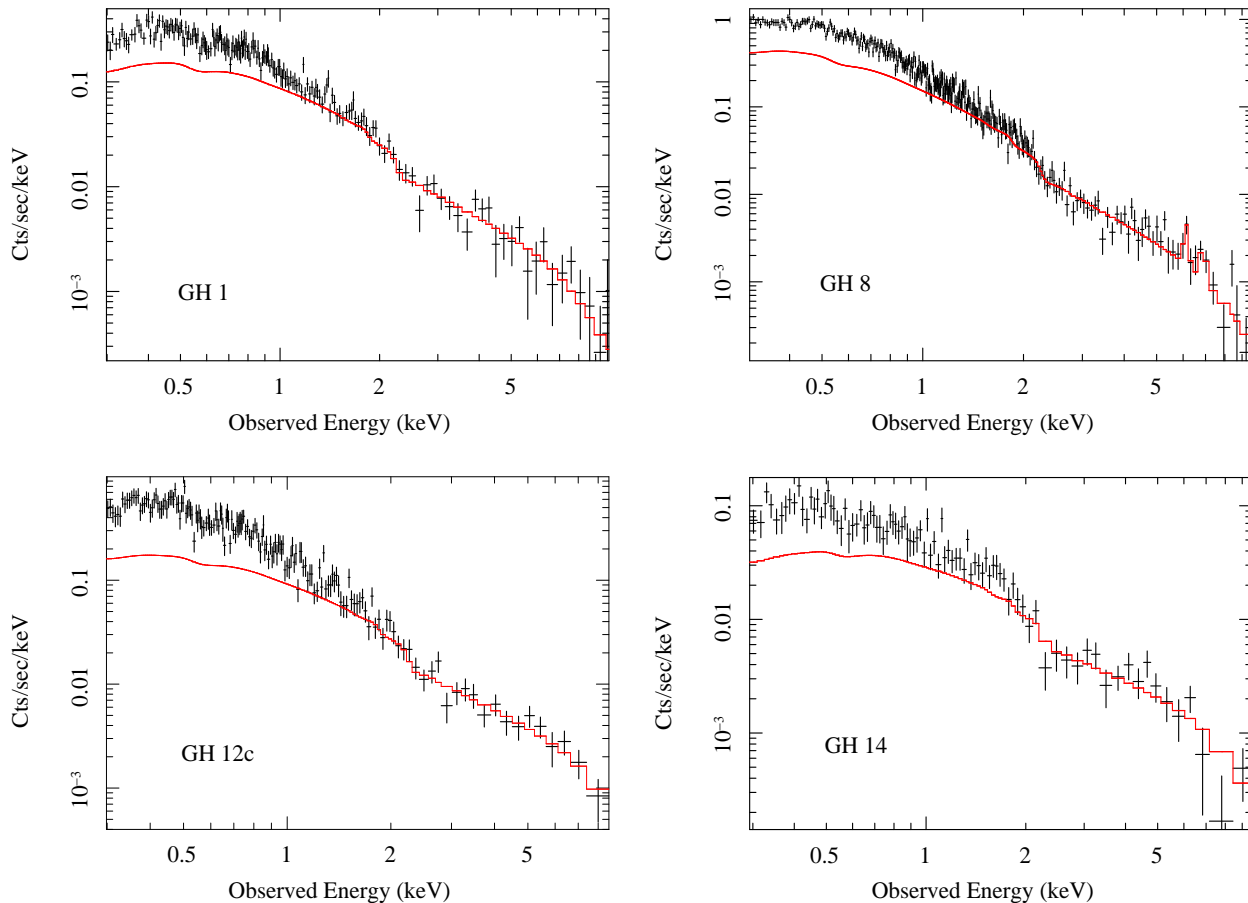


Figure 1. The EPIC-pn spectra of the four objects are shown together with a power law model fitted in the 2–10 keV band only. In all cases, a soft excess is present below 1–2 keV with respect to the extrapolated hard spectral model. For source GH 12, we only show one observation (GH 12c). When a phenomenological blackbody plus power law model is used to fit the spectra (Table 3 and text for details), the improvement with respect to the single power law model is at the >99.99 per cent confidence level in GH 1, GH 8, and GH 12c, 98 per cent in GH 12a, and is not significant in GH 14.

both the soft and the hard bands with respect to the other objects and, as mentioned, is also the only source for which a soft excess is not statistically required. We conclude that the X-ray spectral properties of our small sample of intermediate-mass black hole AGN do not significantly differ from the average properties of luminous AGN powered by accretion onto more massive and more luminous black holes.

4 THE NATURE OF THE SOFT EXCESS

The nature of the soft excess origin in Seyfert 1 galaxies is still unclear and matter of debate. As pointed out by several authors, the idea that the soft excess in AGN represents the high energy tail of the quasi-blackbody emission from the accretion disc is not consistent with the observed properties in luminous samples (Czerny et al 2003; Gierliński & Done 2004; Crummy et al 2006). The maximum temperature for a standard Shakura–Sunyaev thin disc and under the assumption that the energy release is dominated by thermal emission is achieved at the innermost disc radius r_{in} and can be rewritten (e.g. Peterson 1997) as

$$kT_{\text{max}} \simeq 23.8 M_8^{-1/4} (\dot{M}/\dot{M}_{\text{Edd}})^{1/4} (r_{\text{in}}/6 r_g)^{-3/4} \text{eV} \quad (1)$$

where M_8 is the black hole mass in units of $10^8 M_\odot$ and $r_g = GM/c^2$. The minimum possible inner disc radius r_{in} is generally assumed to coincide with the last stable circular orbit of a test particle orbiting the black hole in the equatorial plane and ranges from $1.24 r_g$ to $6 r_g$ (for a maximally rotating Kerr black hole and a non-rotating Schwarzschild one respectively).

For the typical black hole masses and accretion rates of PG quasars and a standard optically thick and geometrically thin accretion disc, one would expect an average maximum disc temperature (kT_{max}) of the order of 20 eV (assuming a Schwarzschild hole), with a dispersion of about one order of magnitude (and even smaller temperatures if the energy release is not completely dominated by thermal emission). However, the observed temperature of the soft excess in PG quasars clusters with very little dispersion around 100–150 eV, too hot and too uniform to be associated with disc emission (Porquet et al 2004; Piconcelli et al 2005; Brocksopp et al 2006). Also, when highly variable sources are examined, the soft excess luminosity does not scale with temperature as expected naively from the Planck law (see e.g. Ponti et al 2006). For the IMBH objects we are considering here, the expected kT_{max} ranges between 80 eV and 110 eV for a Schwarzschild hole (and a factor ~ 3.26 higher for a Kerr black hole), and the blackbody emission should largely enter the soft X-ray regime accessible with our

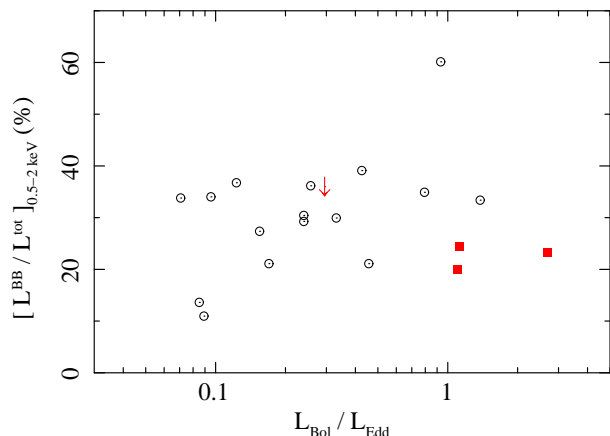


Figure 3. The soft excess strength - defined as the ratio between the BB and the total luminosity in the 0.5–2 keV band - is plotted as a function of Eddington ratio for the radio-quiet PG quasars (open circles) and our four IMBH AGNs (filled squares plus the upper limit). For GH12, the average between observations is shown. No correlation is seen, and the soft excess strength clusters around 30 per cent, though with a large scatter.

XMM–Newton observations, so that the soft X-ray spectra of AGN with IMBH and of (say) PG quasars should significantly differ.

However, as mentioned above, the soft photon index Γ_s we measure is consistent with the average soft photon index in PG quasars, pointing towards a similar spectral shape. This is confirmed when the soft excess in our objects is modeled with a blackbody component. In this case, the inferred temperature turns out to be ~ 100 – 150 eV (see Table 3), remarkably similar to that measured from identical fits to PG quasars (Piconcelli et al 2005). This is shown in Fig. 2 where we plot the observed temperature as a function of the theoretical maximum temperature expected from an accretion disc around a Schwarzschild black hole. Although 100–150 eV is a reasonable value for the disc temperature around our intermediate-mass objects, it is quite remarkable that the inferred temperature is that similar to that of PG quasars, casting doubts on its interpretation in terms of thermal emission, and pointing towards a common and different origin for the soft excess in radiatively efficient black holes of all masses. Moreover, even if all soft X-ray emission is attributed to a thermal disc spectrum, the inferred blackbody luminosity is, for all sources, much lower than the expected one (which can be obtained e.g. by applying the Planck law to Eq. 1). Taking as a representative example GH 12, a blackbody-only fit in the 0.3–0.9 keV band reasonably describes the data ($\chi^2/dof = 250/197$) with a temperature of ~ 137 eV for a total blackbody luminosity of $\sim 1.7 \times 10^{43}$ erg s $^{-1}$, well below that expected one for the given black hole mass and mass accretion rate (in excess of 10^{44} erg s $^{-1}$).

As mentioned above, the only source with no need for a soft excess (GH 14) is also the least luminous, in both absolute and Eddington ratio terms ($L_{\text{Bol}}/L_{\text{Edd}} \sim 0.3$, see Table 2). When fitting the X-ray spectra with a blackbody plus power law model, the strength of the soft excess can be (phenomenologically) defined as the contribution of the blackbody component to the total luminosity in the soft (0.5–2 keV) band. In the case of GH 14, the blackbody contribution is only an upper limit of 36 per cent (Table 3). In order to see if the soft excess is more prominent in higher Eddington ratio sources, we computed the contribution of the blackbody component to the 0.5–2 keV luminosity in a sample of PG quasars (fitting results from Piconcelli et al 2005) and in our intermediate-mass black hole AGN, and we plot it as a function of Eddington

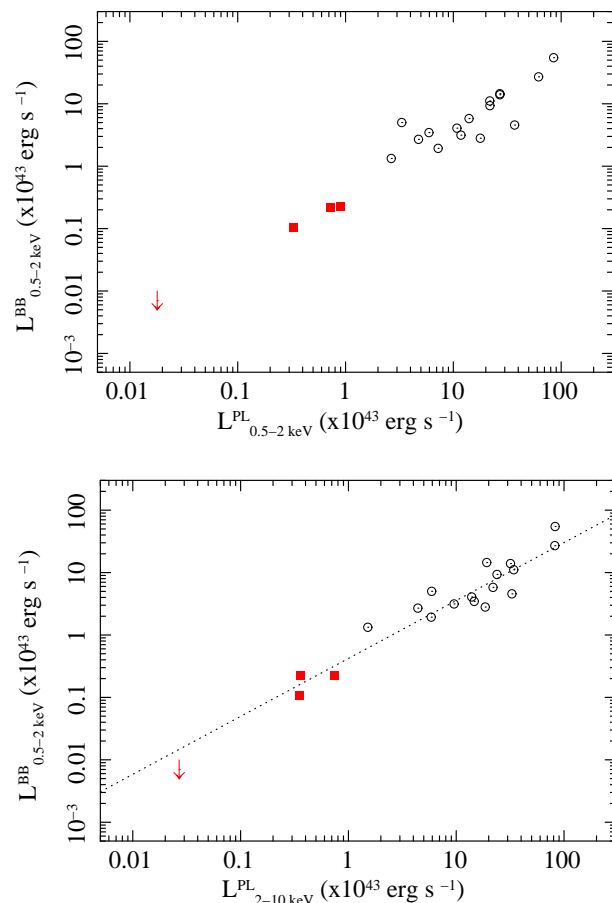


Figure 4. Results from phenomenological BB plus PL fits of the X-ray spectrum for the radio-quiet PG quasars and for our IMBHs (filled squares and upper limit). For GH 12, we plot the average between observations 12a and 12c. In the top panel we show the correlation between the 0.5–2 keV BB luminosity and the PL luminosity in the same band. The BB luminosity is also correlated with the PL luminosity in the hard 2–10 keV band, as shown in the bottom panel ($\log L_{0.5-2 \text{ keV}}^{\text{BB}} = 0.99 \times \log L_{2-10 \text{ keV}}^{\text{PL}}$).

ratio in Fig. 2. As can be seen, no correlation with Eddington ratio is seen, and the blackbody contribution in the 0.5–2 keV band clusters around 30 per cent (although with significant scatter), despite more than one order of magnitude variation in Eddington ratio, i.e. the soft excess strength is nearly uniform in the sample (see e.g. Fig. 4 in Middleton, Done & Gierliński 2007).

The apparent uniform ~ 30 per cent contribution of the soft excess to the soft X-ray luminosity means that the BB and PL luminosities are reasonably well correlated in objects with different black hole mass and mass accretion rate. This is indeed shown in Fig. 3 (top) where we plot the BB luminosity versus the PL one in the 0.5–2 keV band (as inferred from BB plus PL fits to the X-ray spectra of PG quasars, from Piconcelli et al. 2005, and of our IMBH). Although the conversion between the PL 0.5–2 keV and 2–10 keV luminosities depends on the PL slope and is hence object-dependent, it is obvious, that $L_{0.5-2 \text{ keV}}^{\text{BB}}$ is also correlated with the 2–10 keV PL luminosity (see bottom panel of Fig. 3). The good correlation means that the soft excess strength can be used to predict with good accuracy the 2–10 keV luminosity (and vice-versa) implying a physical link between the hard power and the soft excess. Our IMBH are no different from their more massive coun-

Table 3. Results of spectral fits in which the broadband X-ray spectra are modeled with a blackbody (BB) plus power law model (with photon index Γ_h). For GH 14, the soft excess is not statistically required.

BB				
ID	T_{BB}	SE [†] (%)	Γ_h	χ^2/dof
GH 1	0.13 ± 0.01	24.4 ± 6.0	2.05 ± 0.08	293/306
GH 8	0.13 ± 0.01	23.3 ± 4.0	2.5 ± 0.1	346/317
GH 12a	0.11 ± 0.02	16.8 ± 6.0	2.4 ± 0.1	184/206
GH 12c	0.11 ± 0.01	23.0 ± 6.0	2.1 ± 0.1	175/162
GH 14	0.10 ± 0.03	< 36	1.8 ± 0.2	77/88

[†] soft excess (SE) strength in the 0.5–2 keV band: this is the ratio of the BB luminosity to the total one in the 0.5–2 keV band, expressed as a percentage.

terparts and they extend the relationship to lower luminosities (and black hole masses).

4.1 Alternative models I: the smeared absorption model

The universal shape of the soft excess could be better explained if it originated, at least partially, from processes that are genuinely independent from the black hole mass and the AGN luminosity, or accretion rate. Atomic processes can give rise to absorption and emission in the X-ray band affecting the overall spectral shape, and thus provide a possible alternative to optically thick thermal emission as an explanation for the X-ray soft excess.

For instance, Gierliński & Done (2004) proposed a model in which the soft excess is an artifact due to absorption of an underlying simple power law continuum. The model requires a moderately steep intrinsic X-ray continuum ($\Gamma = 2 \div 3$) and absorption by a substantial column of ionized gas, which mostly affects the 0.7–3 keV band, producing an apparent soft excess. Since sharp absorption features are absent in the X-ray spectra, the model also does require very significant smearing which may be due to large velocities of the absorbing gas, as could be found, for instance, in a wind originating from the innermost accretion flow. The model potentially reproduces the X-ray variability properties of some sources (see Gierliński & Done 2006), although flat rms spectra in highly variable sources seem difficult to account for (e.g. during one *XMM-Newton* observations of 1H 0707–495, see Fig. 4 in Boller et al 2003; and also in Mrk 335 see O’Neill et al 2007 and Larsson et al 2008).

When applied to samples of PG quasars and NLS1s, the model provides reasonable spectral fits to the X-ray spectra and requires column densities $N_H \sim 1 \div 5 \times 10^{23} \text{ cm}^{-2}$ with ionization $\log \xi \sim 2.5 \div 3.5$ (Middleton, Done & Gierliński 2007). For the same ionization, larger columns lead to apparent flatter hard spectra so that two sources with identical intrinsic spectrum but different column densities produce very different soft excess strength (in contrast with Fig. 2 and also with Fig. 4 in Middleton, Done & Gierliński 2007).

The only way out for the model to produce a uniform spectral shape and soft excess strength is to force the ionization parameter to be higher for larger column densities, so to reduce the absorption trough and produce a more uniform soft excess strength for different column densities. It is then not surprising that, when the smeared absorption model is fitted to the X-ray spectra of a sample of PG quasars and NLS1 galaxies, a tight correlation between ionization parameter and column density is observed. In Fig. 5 we

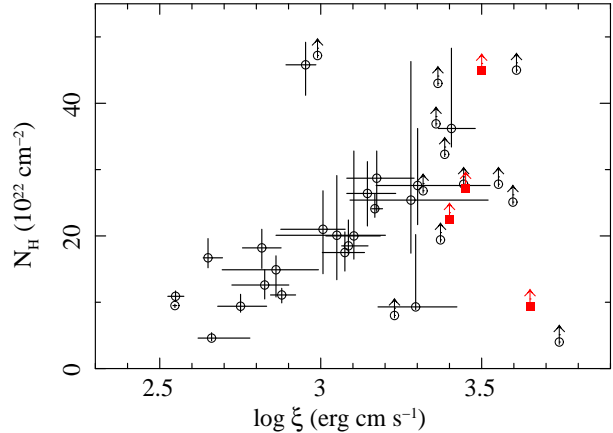


Figure 5. The correlation between column density and ionization parameter as inferred from fitting the smeared absorption model to a sample of PG quasars and NLS1s (open circles results from Middleton, Done & Gierliński 2007) and to our four IMBHs (filled squares, for GH 12 only the first observation is shown for simplicity, see Table 4). Results for which the column density upper limit is equal or larger than the highest tabulated value of $5 \times 10^{23} \text{ cm}^{-2}$ are treated as lower limits at the best-fitting ionization parameter.

show the $N_H - \xi$ correlation as inferred from fitting the model to PG quasars and NLS1s (from Middleton, Done & Gierliński 2007) and to our four IMBHs (results for our objects are reported in Table 4). As mentioned, the correlation of Fig. 5 is most likely produced because the model tries to reproduce the uniform spectral shape and soft excess strength by adjusting the two parameters.

Hence, a question arises: is the $N_H - \xi$ correlation physical in origin, or is it just driven by the model attempting to reproduce the spectral shape by adjusting the parameters in a non physical manner? Simple physical arguments imply that the correlation is not naturally produced: the ionization parameter is defined as $\xi = L/(nr^2)$ where L is the nuclear luminosity, n the absorber density, and r its distance from the nuclear photo-ionizing source. If the absorber is a shell of thickness Δr , then $\xi = L/(rN_H) \Delta r/r$. Since both luminosity and size are expected to roughly scale with the black hole mass, ξ and N_H are naively expected to be anti-correlated (if correlated at all). It is also possible that the correlation seen in Fig 5 is simply due to a degeneracy in the parameter space of the model. If so, and given that the only other parameter (the velocity smearing) is also largely unconstrained (and generally only a lower limit), the model does not provide significant insights on the properties of the absorber (i.e. any column density will be able to provide a good parameterization provided that the ionization state lies on the $N_H - \xi$ correlation of Fig. 5).

4.2 Alternative models II: the disc reflection model

On the other hand, the soft excess universal shape may be due to the presence of an atomic-related emission component rather than absorption. The natural candidate is X-ray reflection from the irradiated accretion disc in which the sharp atomic features (mainly fluorescent emission lines and absorption edges from the most abundant metals) are broadened and smeared out quite naturally because of the high velocities and strong gravity effects in the inner disc. The model has the advantage that such a spectrum has been observed with very little ambiguity in some AGN (see Fabian & Miniutti 2007 for a review) and Galactic X-ray binaries (see Miller 2007 for a review). As the absorption model, disc reflection potentially

Table 4. Results of spectral fits in the 0.3–10 keV band with the two alternative models for the soft excess. *Smeared Absorption*: column densities are given in units of 10^{22} cm^{-2} . The velocity dispersion σ is a free parameter of the model but is not reported here because it is always a lower limit of at least $0.25 c$. *Disc Reflection*: The disc inclination is allowed to vary in the range of $0^\circ - 45^\circ$ only (to be consistent with the Seyfert 1 nature of the sources). The disc extends from the last stable orbit for Schwarzschild or Kerr black holes out to $400 r_g$ and the best-fitting case is reported in the last column (K or S). The emissivity of the reflecting disc is fixed to the standard r^{-3} profile and solar abundances are assumed. In the first column, we report the reflection fraction of the disc reflection component. In the bottom part of the table, we present a model in which we add thermal disc emission to the reflection model (*Disc Reflection + Disc BB*). Though not required statistically with high significance, this solution is more self-consistent than that with reflection only (see text). We use the DISKBB model, and its temperature is set to the maximum one for a Schwarzschild or a Kerr black hole (according to Eq. 1). The geometry is given in parenthesis and represents the best-fitting case from the simultaneous constraints of the thermal and reflection models (we adopt Schwarzschild for GH 14). Part of the soft excess is now described by thermal emission, and we report the ratio of the BB-to-reflection flux in the 0.5–2 keV band for comparison.

Smeared Absorption				
ID	$N_H^{(a)}$	$\log \xi$	Γ	χ^2/dof
GH 1	≥ 27	3.45 ± 0.25	2.11 ± 0.08	301/305
GH 8	≥ 45	3.50 ± 0.20	2.59 ± 0.07	376/316
GH 12a	≥ 22	3.40 ± 0.25	2.45 ± 0.15	178/205
GH 12c	≥ 35	3.52 ± 0.28	2.30 ± 0.19	172/161
GH 14	≥ 10	≥ 3.0	1.80 ± 0.20	76/88
Disc Reflection				
ID	R	$\log \xi^{(b)}$	Γ	χ^2/dof
GH 1	1.2 ± 0.5	1.98 ± 0.25	2.20 ± 0.09	296/305 (K)
GH 8	1.9 ± 0.4	2.48 ± 0.30	2.60 ± 0.14	350/316 (S)
GH 12a	0.9 ± 0.6	2.46 ± 0.35	2.42 ± 0.16	179/205 (K)
GH 12c	1.2 ± 0.6	2.66 ± 0.35	2.20 ± 0.17	177/161 (K)
GH 14	≤ 0.8	–	1.82 ± 0.20	78/88 (K/S)
Disc Reflection + Disc BB				
ID	kT^f	BB/Ref ^(c)	Γ	χ^2/dof
GH 1	0.275	1.63 ± 0.65	2.26 ± 0.11	293/304 (K)
GH 8	0.356	0.23 ± 0.16	2.70 ± 0.18	346/315 (K)
GH 12a	0.255	< 1.90	2.48 ± 0.19	178/204 (K)
GH 12c	0.255	< 1.60	2.30 ± 0.25	173/160 (K)
GH 14	0.083	–	1.82 ± 0.20	77/87 (S)

(a) The highest tabulated value in the model is $N_H = 50 \times 10^{22} \text{ cm}^{-2}$.

Lower limits mean that the parameter could not be constrained below that value. (b) The ionization state of the reflector is unconstrained in GH 14.

(c) The ratio between the BB and the reflection flux in the 0.5–2 keV band is given to compare the contribution of these two components. The ratio and spacetime geometry are unconstrained in GH 14, given that the soft excess itself in this object is an upper limit only.

explains not only the spectral shape, but also the spectral variability properties of many sources (Miniutti & Fabian 2004; Fabian et al 2004; 2005; Ponti et al 2006; Miniutti et al. 2007). The XMM–Newton bandpass is too limited to disentangle statistically between reflection and absorption, which predict different spectral shapes mainly above 10 keV. We provide a comparison in Table 4, showing that the two models are indeed indistinguishable in terms of fitting statistics.

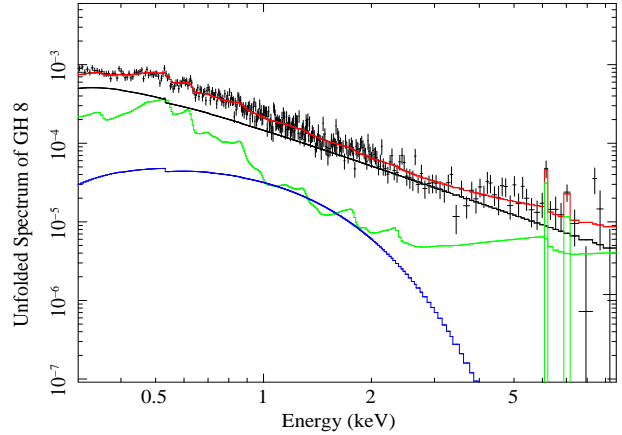


Figure 6. The unfolded spectrum and model components for the Reflection + Disc BB fit of GH 8.

However, the two models differ in their physical interpretation and consequences. The disc reflection model main parameters are i) the ionization state of the reflector and ii) the reflection fraction, i.e. the relative strength of the reflection component with respect to the intrinsic continuum. The inclination of the line of sight with respect to the disc also plays an important role affecting the overall spectral shape (especially if it is larger than 50 degrees), but we assume in the qualitative discussion below that the inclination is smaller for all Seyfert 1 galaxies.

To be successful, the model needs to explain the uniform spectral shape and soft excess strength in different sources by adjusting these parameters in a physically reasonable way. Generally speaking, a larger reflection fraction (for fixed ξ) produces flatter hard spectral shapes (with a similar effect as the increase in column density in the smeared absorption model). Hence, if the ionization parameter stays the same, the model runs into the same problems as the smeared absorption one, and is unlikely to be able to produce a uniform soft excess strength.

However, a correlation between ionization state of the disc and reflection fraction is qualitatively naturally expected in the reflection interpretation. Indeed, a larger reflection fraction means that the continuum irradiates preferentially the disc rather than the observer or, in other words, that the disc subtends a larger solid angle at the X–ray continuum source. The inner disc irradiation is therefore stronger for higher reflection fractions and one expects, for a given disc density, an increase of the ionization of the inner disc.

If we assume that the correlation is linear, i.e. that a doubling of the reflection fraction induces a doubling of the ionization parameter, we can test whether this correlation would give rise to a uniform soft excess. We simulate two 100 ks XMM–Newton spectra which differ in reflection fraction ($R = 1$ and $R = 2$ respectively) and disc ionization ($\xi = 250 \text{ erg cm s}^{-1}$ and $\xi = 500 \text{ erg cm s}^{-1}$ respectively). By fitting the two spectra with a blackbody plus power law model, we obtain a soft excess strength of ~ 22 and ~ 30 per cent respectively, in line with the spread and absolute value observed in Fig. 2. In other words, doubling the reflection fraction and the ionization parameter only produces a marginal increase in the soft excess strength, fully consistent with the observed spread.

4.2.1 Adding the disc thermal emission component

In contrast with the case of large black hole mass AGN where thermal disc emission is in the UV, for the black hole masses and ac-

cretion rates (Tables 1 and 2) of our mini-sample of IMBHs, it should significantly contribute at soft X-ray energies especially if the disc extends down to its last stable orbit around the black hole (see Eq. 1). Then, even if reflection alone can account for all the soft excess, a self-consistent model should also include thermal disc emission. We then added a disc blackbody component (the multi-color DISKBB model) with temperature fixed to that expected from the standard thin disc model (Eq. 1) in the two extreme cases of Schwarzschild and maximally spinning Kerr geometries. The relativistic blurring of the reflection component is self-consistently computed according to the two spacetime geometries and we report results for the best-fitting geometry only. In one case (GH 8), the addition of the thermal component suggests a change (from Schwarzschild to Kerr) of the best-fitting geometry. The results are presented in the bottom part of Table 4 and show that, though not required formally by the data, a thermal disc component with the right temperature is consistent with the X-ray spectra of our IMBHs, even when the reflection component is introduced.

We point out however that the inferred blackbody luminosity is again (see Section 4) far below that expected from accretion theory. This is not completely surprising given that the estimate in Eq. 1 assumes, by definition, that all of the accretion energy release is in the form of a thermal component, i.e. that the expected blackbody luminosity is comparable to the bolometric. This may be accurate for BH binaries in disc-dominated (or soft) states, but in the present case of small black hole mass AGN, and even if the thermal component should dominate the soft X-rays, much of the X-ray emission is clearly not in the form of a thermal component, which makes it difficult to predict reliably the expected blackbody temperatures and luminosities. It should also be stressed that the low inferred blackbody luminosity is not an artifact of the presence of the reflection component eating away part of the soft excess. Even if the soft excess is modelled entirely as a blackbody, its total unabsorbed luminosity is in all of our sources more than one order of magnitude below the expected one (see Section 4). To illustrate the relative contribution of the thermal (blue) and reflection (green) components, we show the unfolded spectrum and model components for the case of GH 8 in Fig. 6.

5 X-RAY VARIABILITY

One of the main goals of our *XMM-Newton* observations was to search for X-ray variability in our mini-sample of IMBHs. Since the BH mass sets the geometrical scale of the system, and since X-rays are thought to originate in the innermost few tens gravitational radii, short timescale variability has to be expected from our IMBH sample. As a reference, the light crossing time of a sphere of $50 r_g$ in radius is ~ 500 s for a $10^6 M_\odot$ BH. Hence, X-ray variability down to a few hundred seconds (at least) has to be expected for our sources if, as generally assumed, the X-ray emission in AGNs originates in the innermost regions of the accretion flow.

In Fig. 7 we show the broadband (0.2–10 keV) background subtracted light curves for all our objects with a 200 s time-bin, as obtained from the EPIC pn data. X-ray variability is clearly detected in all cases down to the bin-size timescale, confirming that the X-ray emitting region must be compact, of the order of a few tens of gravitational radii.

One of the most powerful ways to investigate the nature and properties of X-ray variability (and any time-series) is the analysis of the power spectral density (PSD), i.e. the distribution of the power of the signal as a function of frequency. At least one charac-

teristic frequency (or timescale) can be derived from the PSD of accreting black hole X-ray light curves. If the PSD is parameterized as $P(\nu) \propto \nu^{-\alpha}$, most AGN and X-ray binaries in the high/soft state have $\alpha \approx 2$ which breaks to $\alpha \approx 1$ below a characteristic high frequency break ν_H . In addition to the high frequency break, X-ray binaries in the hard and intermediate states also exhibit a second low frequency break ν_L and, for frequencies below ν_L , the PSD slope becomes $\alpha \approx 0$. For AGN, convincing evidence for a low frequency break has been reported in Ark 564 only (McHardy et al 2007).

5.1 Excess variance

In the case of our IMBH observations, the data quality is not high enough to accurately measure the PSD shape and test for the presence of reliable high frequency breaks. However, a comparison between the IMBH X-ray variability and that of more massive AGN can be obtained by the analysis of the so-called excess variance σ_{NXS}^2 , which is the integral of the power spectrum over a given frequency window $\Delta\nu$, defined by the light curve duration and time-bin (Nandra et al 1997; Edelson et al 2002; Vaughan et al 2003).

Early results pointed out an anti-correlation between excess variance and AGN luminosity (Green, McHardy & Letho 1993; Lawrence & Papadakis 1997; Nandra et al 1997). Later study by Lu & Yu (2001) however outlined an underlying anti-correlation between σ_{NXS}^2 and black hole mass on variability timescales of ~ 1 day, a result later extended to longer timescales by Papadakis (2004). More recently, O’Neill et al (2005) have computed σ_{NXS}^2 for a large sample of AGN of known black hole mass observed with *ASCA*, confirming the general anti-correlation seen before, and pointing out that the observed behaviour can be explained by assuming a universal form of the PSD with both a low and a high frequency break and by further assuming that the PSD amplitude is uniform (i.e. the same in all sources) and that the frequency breaks (most notably ν_H) are proportional to M_{BH}^{-1} (see e.g. Papadakis 2004; Markowitz et al 2003; O’Neill et al 2005). While such model reproduces the σ_{NXS}^2 – M_{BH} relationship well, the scatter in the relationship is too large to compute errors on the parameters (O’Neill et al 2005). In fact, it must be stressed that the above assumptions are only zeroth-order approximations because the PSD amplitude is known to vary significantly from source to source (e.g. Uttley & McHardy 2005) and ν_H has been convincingly shown to be not only a function of the black hole mass, but also of the accretion rate (McHardy et al 2006). Moreover, the low-frequency break ν_L affects the low-mass end curvature in the relationship but is most likely outside the observable frequency window for typical X-ray observations of AGN with the exception of Ark 564; McHardy et al. (2007), and one object only is clearly not enough to infer the general scaling between the low and high frequency breaks in AGN.

Because of the above limitations, it is not our purpose here to repeat the O’Neill et al analysis (as we cannot constrain the parameters of the model any better), but in order to compare the IMBH variability properties with more massive objects, we consider a sample of 27 radio-quiet Seyfert 1 galaxies observed with *XMM-Newton* plus our 4 IMBHs and compute the excess variance by using light-curve segments of equal duration ($T = 20$ ks) and equal time bin size ($\delta T = 500$ s) in the 2–10 keV band for all sources. The sample was selected from the available sources (with known/estimated black hole mass) in the *XMM-Newton* public archive with observations longer than 20 ks. The sample is by no means homogeneous nor complete and results are reported here for comparison with the IMBH only. If observations longer than

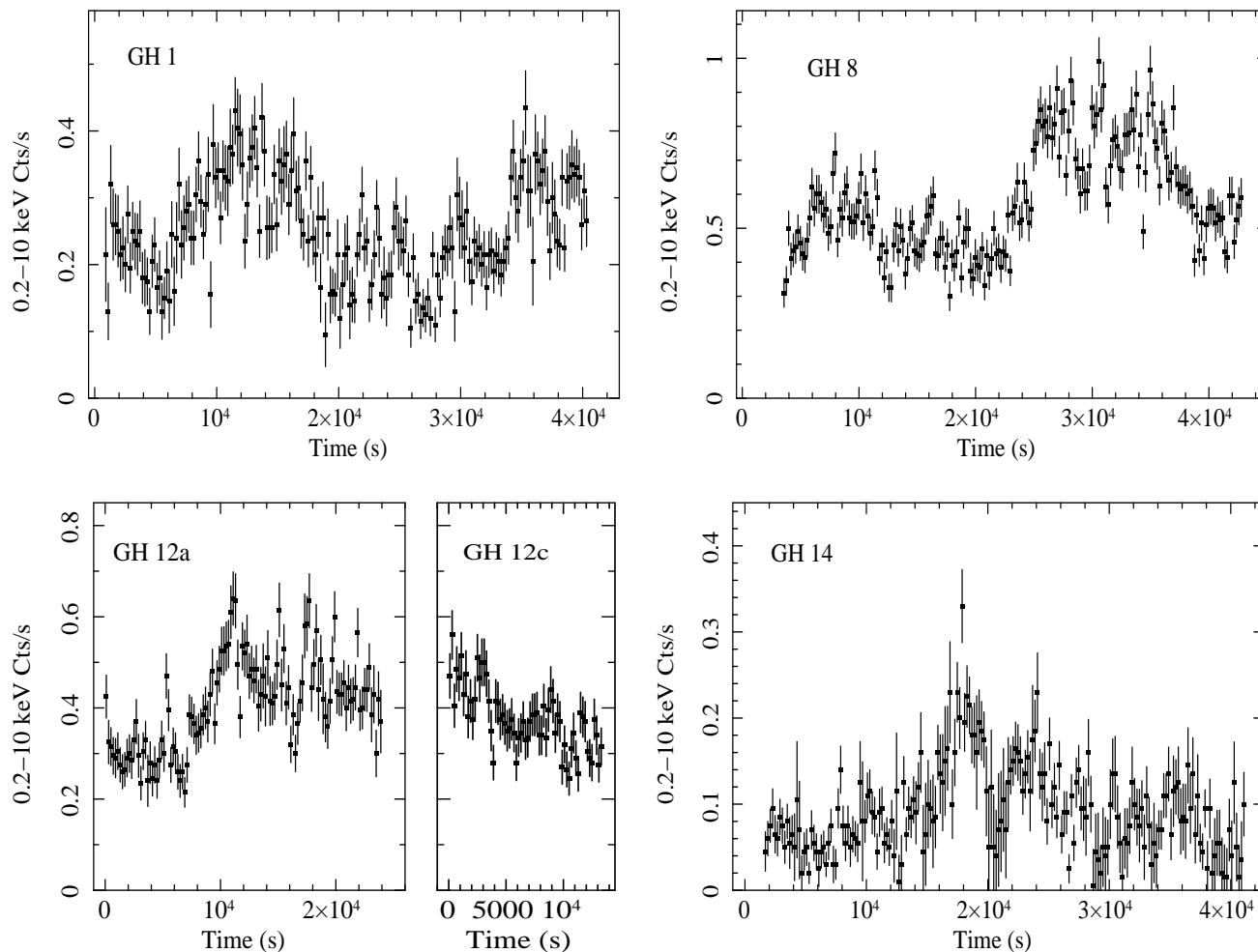


Figure 7. Background-subtracted 0.2–10 keV EPIC pn light curves for the four objects (common time bin size of 200 s). For GH12, we show the light curves from the longest GH12a and GH12c (69 d apart) observations only (during the shorter GH 12b observation, the mean count rate is ~ 0.5 Cts/s).

20 ks (or multiple observations) are available for a given source, the excess variance has been estimated as the mean over the excess variances obtained from the 20 ks intervals and errors are computed taking into account the measurement errors, and also the uncertainties associated with red-noise (Vaughan et al. 2003). In the case of GH 12, we used observation GH 12a only, and we imposed a slightly less conservative background cut than for the spectral analysis in order to obtain a 20 ks segment of the 2–10 keV light curve (we checked that the different cut does not affect the excess variance significantly).

The excess variances and black hole masses used here are reported in Table 5. In Fig. 8, we show the resulting $\log \sigma_{\text{NXS}}^2 - \log M_{\text{BH}}$ relationship, showing that the excess variance of our IMBHs (filled squares) smoothly joins with that of more massive sources. Such behaviour is consistent with that generally predicted by the universal PSD model, although with the model limitations discussed above (see e.g. Fig. 2 in O’Neill et al 2005) and we conclude that the IMBH X-ray variability properties do not differ significantly from those of more massive Seyfert galaxies. Only extending the available data to black hole masses below $\sim 10^5 M_{\odot}$ would better define the relationship in the most crucial low-mass end where, according to the universal PSD model, the excess variance is expected to significantly deviate from the anti-correlation

(and actually to nearly saturate if, as results from Ark 564 indicate, the low frequency break in AGN is $\nu_{\text{L}} \leq 10^{-3} \times \nu_{\text{H}}$).

6 DISCUSSION

We have observed with *XMM-Newton* 4 IMBH from the original sample of 19 objects selected by Greene & Ho (2004) from the SDSS. The X-ray properties of the IMBH considered here do not significantly differ from those of their more massive counterparts such as the PG quasars. The IMBHs could represent a population of not yet fully grown super-massive black holes and, if in a rapid growing phase, their accretion properties would be expected to significantly depart from those of standard and fully-grown accreting supermassive black holes. However, as already suggested by their Eddington ratios (high because of the sample selection strategy, but not that unusual), their accretion properties are in all respect similar to those of more massive AGN and quasars.

The X-ray spectra of our objects are characterized by the same X-ray slope as PG quasars in both the hard and soft X-ray bands. No (neutral) absorption in excess of the Galactic one is observed in any of the objects. Three out of four objects exhibit a soft excess with the same properties (uniform temperature and strength)

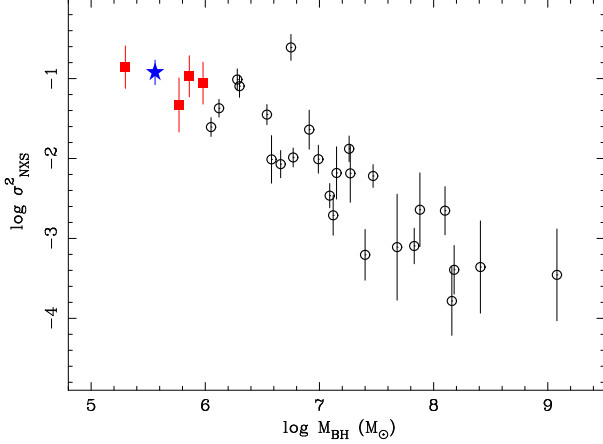


Figure 8. Top: Excess variance as a function of black hole mass. Filled squares represent our mini-sample of IMBHs, the filled star is NGC 4395, and open circles for a sample of radio-quiet Seyfert 1 galaxies observed with *XMM-Newton* (see Table 5 and text for details).

Table 5. Black hole mass and excess variance for a sample of 27 radio quiet Seyfert 1 galaxies (including also NLS1 galaxies and 1 IMBH, e.g. NGC 4395) and for our 4 IMBH.

ID	$\log M_{\text{BH}}$	$\log \sigma_{\text{NXS}}^2$	Ref [†]
GH 1	5.86	-0.97 ± 0.26	[1]
GH 8	5.77	-1.33 ± 0.34	[1]
GH 12	5.98	-1.06 ± 0.26	[1]
GH 14	5.30	-0.86 ± 0.27	[1]
NGC 4395	5.56	-0.92 ± 0.15	[2]
Mrk 766	6.05	-1.61 ± 0.12	[3]
Ark 564	6.12	-1.37 ± 0.11	[4]
NGC 4051	6.28	-1.01 ± 0.13	[5]
1H 0707-495	6.30	-1.10 ± 0.14	[3]
MCG-6-30-15	6.54	-1.45 ± 0.13	[6]
MS 2254-36	6.58	-2.01 ± 0.30	[7]
WAS 61	6.66	-2.07 ± 0.17	[7]
IRAS 13224-3809	6.75	-0.61 ± 0.16	[3]
IC 4329A	6.77	-1.99 ± 0.12	[8]
TonS 180	6.91	-1.64 ± 0.24	[3]
NGC 4593	6.99	-2.01 ± 0.18	[9]
NGC 7469	7.09	-2.46 ± 0.15	[5]
NGC 4151	7.12	-2.71 ± 0.25	[5]
Mrk 335	7.15	-2.18 ± 0.33	[5]
IZw1	7.26	-1.88 ± 0.16	[3]
Mrk 478	7.27	-2.19 ± 0.36	[3]
Mrk 110	7.40	-3.21 ± 0.32	[5]
NGC 3783	7.47	-2.21 ± 0.14	[5]
Mrk 590	7.68	-3.11 ± 0.66	[5]
NGC 5548	7.83	-3.09 ± 0.22	[5]
PG 1211+143	7.88	-2.64 ± 0.46	[3]
Mrk 841	8.10	-2.65 ± 0.30	[8]
Mrk 509	8.16	-3.78 ± 0.43	[5]
Ark 120	8.18	-3.39 ± 0.31	[5]
Fairall 9	8.41	-3.36 ± 0.58	[5]
HE 1029-1401	9.08	-3.46 ± 0.57	[3]

[†] References for black hole masses are: [1] Greene & Ho (2004); [2] Peterson et al (2005); [3] Wang et al. (2004); [4] Botte et al. (2004); [5] Peterson et al. (2004); [6] McHardy et al. (2005); [7] Grupe et al. (2004); [8] Woo & Urry (2002); [9] Denney et al. (2006)

as larger black hole mass samples (standard Seyfert 1 and quasars). This is surprising if one considers that the small black hole mass of the IMBHs should allow thermal emission from the accretion disc to dominate the soft X-ray band, producing soft X-ray spectra that should significantly depart from those of more massive objects in which the disc quasi-blackbody emission is expected to contribute in the UV only. This is however not observed, and if the soft excess is interpreted as thermal disc emission, the inferred temperature in AGN with black hole masses of $\leq 10^6 M_{\odot}$ is the same as that of quasars with black hole masses two (or more) orders of magnitude larger. So far, the so-called soft excess problem was mainly defined as the fact that we observe soft X-ray emission in accreting supermassive black hole which is too hot (and too uniform) to be reasonably associated with thermal disc emission. Here, we point out that the problem is even more puzzling: when we observe sources in which thermal disc emission should largely extend into the soft X-ray band (such as the IMBH), we see exactly the same spectral shape as in more massive AGN and, if these IMBH were rotating (Kerr), the inferred temperature would even be too cold to be associated with the accretion disc.

6.1 Smearing absorption

Gierliński & Done (2004) proposed that the soft excess is an artifact due to absorption (of an intrinsic steep power law spectrum) by partially ionized gas in the form of a highly relativistic wind. Since the observed smoothness of the soft excess is not consistent with the expected sharp absorption features, the model requires the gas to be characterized by strong velocity gradients to smear them out via Doppler smearing. The large velocity gradients, most likely imply that the wind is launched very close to the black hole.

As mentioned by Schurch & Done (2006), the wind model described above is unlikely to be a standard UV-line driven disc wind, because such winds are preferentially produced at $i > 75^{\circ}$ of the axis, which is in contrast with the observational fact that most low-inclination Seyfert 1 galaxies exhibit a soft excess. Moreover, the mass outflow rate (\dot{M}_{out}) inferred from the large final velocities required by the model is generally hundreds times larger than the mass accretion rate (\dot{M}_{acc}) in among the most luminous X-ray sources in the Universe (but see the idea of a failed wind proposed by Schurch & Done 2006). More recently, Schurch & Done (2007) have shown that when a more detailed smearing profile is adopted, the shape of the model does not describe well the observed smoothness of the soft excess, casting severe doubts on the overall model.

In addition, here we have shown that, even if the smeared absorption model can reproduce the spectral shape, the uniform soft excess strength is obtained only if a tight correlation between column density and ionization parameter is enforced. The $N_{\text{H}} - \xi$ correlation inferred from fitting the smeared absorption model to X-ray data is however not a natural product of photo-ionization and is most likely spurious, either due to a degeneracy in the parameter space (which implies the model does not provide any constraint on the absorber properties) or, as mentioned above, to the need of producing a uniform soft excess strength in sources which do require different column densities.

6.2 Disc reflection

The smearing of the reflection features by high velocities is a natural consequence of the presence of an inner accretion disc. Undoubtedly, an inner accretion disc must exist in sources accreting

above a few per cent of the Eddington ratio and thus, unlikely the smeared absorption model, the disc reflection model does not introduce any new (so far unobserved, if not for the soft excess interpretation itself) component to explain the soft excess. The reflection interpretation just makes use of the basic ingredients of accretion theory, a powerful primary source of hard X-rays, and an optically thick accretion disc which reprocesses the irradiating flux into a reflection spectrum. An additional external absorber may obviously mask this contribution and this may well be the case in some most extreme sources. However, since disc reflection only requires the presence of an inner accretion disc and of an illuminating X-ray source, it is an unavoidable component in any reasonable accretion model for radiatively efficient AGN (and X-ray binaries). In fact (see e.g. Middleton, Done & Gierliński 2007) when the smeared absorption model is applied to PG quasars and NLS1s, it always does require also a disc reflection component. If the disc reflection component alone can account for the spectral shape and variability of the sources, it is difficult to understand the need for an additional smeared absorber with problematic launching mechanism, extreme mass outflow rate, and rather unnatural relationship between column density and ionization.

Since disc reflection invokes the presence of the accretion disc down to the last stable orbit, thermal emission from the disc should also be present and, given the small black hole masses and relatively high accretion rates in our IMBHs, such emission should peak in the soft X-rays. Indeed, when a multicolor disc blackbody is included in the spectral models, a solution in which the soft excess is partly due to reflection and partly to disc blackbody with the theoretically expected temperature is found. However, we point out that if thermal disc emission is present in the soft X-ray spectrum of these objects, its luminosity is far below the expected one for the given temperatures not only when reflection is invoked, but even when all the soft excess is modelled as a pure disc blackbody.

It is actually difficult to distinguish between the two competing models (smeared absorption and disc reflection) by using spectral and variability information in the limited band-pass of XMM–Newton (0.3–10 keV band) even in bright, well observed sources. Moreover, our mini-sample of small mass BH is not well suited to investigate the problem due to the relatively low quality of the data. High-energy data are crucial to test whether the X-ray spectrum above 10 keV is just the high-energy unabsorbed tail of the intrinsic power law continuum, or whether it is instead characterized by the presence of a Compton hump around 20–30 keV, related to X-ray reflection. While signatures for the presence of X-ray reflection from the inner accretion disc are sometimes detected, the number of well observed sources above 10 keV is still too small to draw any clear-cut conclusion (e.g. Miniutti et al 2007; Reeves et al 2007). Observations with the *Suzaku* X-ray mission and with future missions such as *Simbol-X* (Ferrando et al. 2006) will most likely play a crucial role in that direction in the near future.

6.3 X-ray variability

Given their relatively small black hole mass (i.e. small size), the observed IMBH are not surprisingly among the most variable in X-rays. In particular, their excess variance σ_{NXS}^2 is among the largest obtained from AGN X-ray light curves. Our observations begin to fill a relatively poorly explored range of black hole masses in the σ_{NXS}^2 – M_{BH} relationship and show that the X-ray variability properties of IMBH smoothly join with those of more massive Seyfert galaxies. The σ_{NXS}^2 – M_{BH} is consistent with a simple (well known) anti-correlation that can be explained with a universal PSD

model in which the break frequencies (most importantly the high-frequency one) scale with M_{BH}^{-1} . However, such functional form for ν_{H} is known to be only a zeroth-order approximation (see M^cHardy et al 2006) and the universal PSD model suffers also for other uncertainties that do not allow to properly account for the scatter in the relationship. Future longer observations of these and other IMBH in X-rays would allow to explicitly search for the high frequency break in the PSD, enabling us to extend the ν_{H} – M_{BH} – \dot{M}_{acc} relationship pointed out by M^cHardy et al (2006) to the most crucial black hole mass range of $M_{\text{BH}} \leq 10^6 M_{\odot}$.

ACKNOWLEDGMENTS

Based on observations obtained with XMM–Newton, an ESA science mission with instruments and contributions directly funded by ESA Member States and NASA. We would like to thank the referee for her/his suggestions that improved our work. GM thanks the UK STFC and the French CNRS for partial support. GM also thanks the Spanish Ministerio de Ciencia e Innovación and CSIC for support through a Ramón y Cajal contract. ACF thanks the Royal Society for support.

REFERENCES

- Barth A.J., Ho L.C., Rytledge R.E., Sargent W.L.W., 2004, ApJ, 607, 90
- Bianchi S., Guainazzi M, Matt G., Fonseca Bonilla N., 2007, A&A, 467, L19
- Boller Th. et al, 2003, MNRAS, 329, L1
- Botte V., Ciroi S., Rafanelli P., di Mille F., 2004, AJ, 127, 3168
- Brocksopp C., Starling R.L.C., Schady P., Mason K.O., Romero-Colmenero E., Puchnarewicz E.M., 2006, MNRAS, 366, 953
- Crummy J., Fabian A.C., Gallo L., Ross R.R., 2006, MNRAS, 365, 1067
- Czerny B., Nikołajuk M., Róžańska A., Dumont A.-M., Loska Z., Życki P.T., 2003, A&A, 412, 317
- Denney K.D. et al., 2006, ApJ, 653, 152
- Dewangan G.C., Mathur S., Griffiths R.E., Rao A.R., 2008, submitted to ApJ (preprint arXiv:0801.3663)
- Done C., Gierliński M., 2005, MNRAS, 364, 208
- Dong X. et al., 2007a, ApJ, 657, 700
- Dong X. et al., 2007b, Proc. of “The Central Engine of Active Galactic Nuclei”, eds. L.C. Ho, J.-M. Wang, 2007, ASP Conference Series, 373, 57
- Edelson R., Turner T.J., Pounds K., Vaughan S., Markowitz A., Marshall D., Dobbie P., Warwick R.S., 2002, ApJ, 568, 610
- Fabian A.C., Miniutti G., Gallo L., Boller Th., Tanaka Y., Vaughan S., Ross R.R., 2004, MNRAS, 353, 1071
- Fabian A.C., Miniutti G., Iwasawa K., Ross R.R., 2005, MNRAS, 361, 795
- Fabian A.C., Miniutti G., 2007, in “Kerr Spacetime: Rotating Black Holes in General Relativity” eds. D.L. Wiltshire, M. Visser and S.M. Scott, Cambridge Univ. Press in press (preprint astro-ph/0507409)
- Ferrando P. et al, 2006, in *Space Telescopes and Instrumentations II: Ultraviolet to Gamma Ray*, eds: Turner M.J.L., Hasinger G., Proc. of the SPIE, 6266, 62660F
- Filippenko A.V., Ho L.C., Sargent W.L.W., 1993, ApJ, 410, L75
- Filippenko A.V., Ho L.C., 2003, ApJ, 588, L13
- Gebhardt K., Rich R.M., Ho L.C., 2005, ApJ, 634, 1093

- Gierliński M., Done C., 2004, MNRAS, 349, L7
 Gierliński M., Done C., 2006, MNRAS, 371, L16
 Green A.R., M^cHardy I.M., Letho H.J., 1993, MNRAS, 265, 664
 Greene J.E., Ho L.C., 2004, ApJ, 610, 722
 Greene J.E., Ho L.C., 2007a, ApJ, 656, 84
 Greene J.E., Ho L.C., 2007b, ApJ, 670, 92
 Grupe D., Wills B.J., Leighly K.M., Meusinger H., 2004, AJ, 127, 156
 Ho L.C., Ulvestad J.S., 2001, ApJS, 133, 77
 Ho L.C. et al., 2001, ApJ, 549, L51
 Kunth D., Sargent W.L.W., Bothun G.D., 1987, AJ, 93, 29
 Larsson J., Miniutti G., Fabian A.C., Miller J.M., Reynolds C.S., Ponti G., 2008, MNRAS, 384, 1316
 Lawrence A., Papadakis I., 1993, ApJ, 414, L85
 Lu Y., Yu Q., 2001, MNRAS, 324, 653
 Markowitz A. et al, 2003, ApJ, 593, 96
 M^cHardy I.M., Gunn K.F., Uttley P., Goad M.R., 2005, MNRAS, 359, 1469
 M^cHardy I.M., Koerding E., Knigge C., Uttley P., Fender R.P., 2006, Nature, 444, 730
 M^cHardy I.M., Arèvalo P., Uttley P., Papadakis I.E., Summons D.P., Brinkmann W., Page M.J., 2007, MNRAS, 382, 985
 Middleton M., Done C., Gierliński M., 2007, MNRAS, 381, 1426
 Miller J.M., 2007, ARA& A, 45, 441
 Miniutti G., Fabian A.C., 2004, MNRAS, 349, 1435
 Miniutti G. et al, 2007, PASJ, 59, SP1, 315
 Nandra K., George I.M., Mushotzky R.F., Turner T.J., Yaqoob T., 1997, ApJ, 476, 70
 Noyola E., Gebhardt K., Bergmann M, 2008, ApJ in press (preprint arXiv:0801.2782)
 O'Neill P.M., Nandra K., Papadakis I., Turner J.T., 2005, MNRAS, 358, 1405
 O'Neill P.M., Nandra K., Cappi M., Longinotti A., Sim S.A., 2007, MNRAS, L94
 Papadakis I., 2004, MNRAS, 348, 207
 Peterson B.M., "An introduction to active galactic nuclei", 1997, NY Cambridge Univ. Press, Cambridge
 Peterson B.M. et al, 2004, ApJ, 613, 682
 Peterson B.M. et al., 2005, ApJ, 632, 799
 Piconcelli E., Jimenez-Bailón E., Guainazzi M., Schartel N., Rodríguez-Pascual P.M., Santos-Lleó M., 2005, A&A, 432, 15
 Ponti G., Miniutti G., Cappi M., Maraschi L., Fabian A.C., Iwasawa K., 2006, MNRAS, 368, 903
 Porquet D., Reeves J.N., O'Brien P., Brinkmann W., 2004, A&A, 422, 85
 Reeves J.N. et al, 2007, PASJ, 59, SP1, 301
 Schurch N.J., Done C., 2007, MNRAS, 381, 1413
 Uttley P., M^cHardy I.M., Papadakis I., 2002, MNRAS, 332, 231
 Uttley P., M^cHardy I.M., 2005, MNRAS, 363, 586
 Vaughan S., Edelson R., Warwick R.S., Uttley P., 2003, MNRAS, 345, 1271
 Vaughan S., Iwasawa K., Fabian A.C., Hayashida K., 2005, MNRAS, 356, 524
 Wang J.-M., Watarai K.-Y., Minieshige S., 2004, ApJ, 607, L107
 Woo J.-H., Urry C.M., 2002, ApJ, 579, 530